IEEE Access
Multidisciplinary | Rapid Review | Open Access Journal

Received November 20, 2017, accepted December 24, 2017, date of publication January 10, 2018,
date of current version March 12, 2018.

Digital Object Identifier 10.1109/ACCESS.2018.2791582

An Automated Calibration Method of Ultrasonic Probe Based on Coherent Point Drift Algorithm

LIFENG WANG[1], TIANMIAO WANG[1,3], HONGPENG LIU[1], LEI HU[1,3], ZHONGHAO HAN[1], WENYONG LIU[2,3], NA GUO[1], YANSONG QI[4], AND YONGSHENG XU[4]

[1]School of Mechanical Engineering and Automation, Beihang University, Beijing 100183, China
[2]School of Biological Science and Medical Engineering, Beihang University, Beijing 100183, China
[3]Beijing Advanced Innovation Centre for Biomedical Engineering, Beihang University, Beijing 100183, China
[4]Department of Orthopedics, Inner Mongolia Peoples' Hospital, Hohhot 010017, China

Corresponding author: Wenyong Liu (wyliu@buaa.edu.cn)

This work was supported in part by the National Hi-Tech Research and Development Program of China (863 Program) under Grant 2015AA043204, in part by the National Natural Science Foundation of China under Grant 61333019 and Grant 81560374, in part by Beijing Natural Science Foundation under Grant Z170001, and in part by the National Science and Technology Major Project of China under Grant 2014ZX04013011.

ABSTRACT Ultrasound-based navigation, as a non-invasive and non-radiation image guiding system, is becoming a research focus in minimally invasive navigation surgery, and calibration between an ultrasonic probe and a 3D vision device is one of the key technologies for ultrasonic registration-based navigation. In this paper, a phantom model was designed as a benchmark for calibration. Both iterative closet point (ICP) and coherent point drift (CPD) algorithms are chosen as point cloud registration methods to implement calibration between ultrasonic scanned points and original phantom points to set up the relationship between the ultrasonic probe and the 3D vision device. Because of large topological difference between the ultrasound scanned points and the points from model, ICP algorithm cannot complete the registration, but the CPD algorithm could implement the registration automatically. The average errors of the center point position for each cavity were 1.50, 1.31, and 1.19 mm, respectively, and the average errors of the axis for each cavity were 0.85°, 0.61°, and 0.99°, respectively. Experiment results showed that the average error of calibration by this method satisfies acquirements of most orthopedic surgeries, and the fully automatic implementation of ultrasonic image processing and subsequent calculation is suitable for on-line calibration and verification in surgery.

INDEX TERMS Coherent point drift, point cloud-based registration, ultrasound probe calibration.

I. INTRODUCTION

One of the key steps in the computer-aided orthopedic surgery (CAOS) is to establish relationship between the preoperative three-dimensional (3D) CT images and the tracking system in surgery, so as to facilitate the real-time tracking of bone trauma during the operation procedure.

Researchers have developed several methods for image-based intraoperative registration. For example, it is common to collect point cloud data of bone surface using probe with visual tracking and then perform an iterative closet point (ICP) registration between the points of bone surface and the 3D points in preoperative CT [1]–[3]. This method has advantages for open surgeries such as joint replacement, but causes additional trauma in minimally invasive surgeries such as fracture reduction and intramedullary nail insertion. Another method achieves navigation based on mapping between two X-ray images (AP and lateral views) or based on registration between X-ray and preoperative CT [4]–[7]. The main disadvantage of this method is that the patients have to be exposed to massive radiation, thus it will reduce the efficiency and potentially threat the health of surgeon and patient. Also, the relation between visual space and CT space can be established using intraoperative CT [8]. This method has high registration accuracy and a high operating efficiency, but rarely deployed in clinical use because of the high price and excessive radiation of intraoperative CT device.

Compared with CT and X-ray, ultrasound has many advantages, such as portability, low cost and no radiation. Therefore, the navigation technology based on ultrasonic registration is becoming a research focus in minimally invasive navigation surgery. Ultrasound-based registration achieves space calibration through registering with

preoperative CT/MRI image. In this research field, many investigators have studied applications of intraoperative ultrasound (A-mode or B-mode) and preoperative CT / MRI registration. In the field of A-mode ultrasound, existed researches suggest ultrasonic detection is accurate enough for CAOS [9], [10]. Moreover, position tracking device is combined with A-mode ultrasound, then landmarks of the skull is detected with an ultrasonic device, at last the same mark is probed with a mechanical probe. A calibrated and registration platform based on A-mode ultrasound was designed and the cadaver test was finished on MAKO robot platform through replacing probe [11]. As B-mode ultrasound can only provide two-dimensional (2D) section image of the body, waveform images of A-mode ultrasound, are less intuitive than B-mode ultrasound 2D images, and clinical use of A-mode ultrasound is now rare because of their poor visibility.

In the field of B-mode ultrasound, 3D imaging technique combining 2D imaging with 3D tracking system (3D visual device) draws more focus recently. Solutions for automatic extraction of bone surface from ultrasound images were investigated in [12]–[14], and experiments on the pelvis and femur of cadaveric bones were conducted through rigidly attaching B-mode ultrasound probe on optical positioning device [15], [16]. One of the key technologies for ultrasonic registration-based navigation is calibration between ultrasonic probe and 3D vision device. As ultrasonic probe is sealed, it is hard to measure externally the transformation matrix of coordinate systems between visual reference frame and ultrasonic image. Only calibration can be used for determining coordinate transformation relationship between visual reference frame and ultrasonic pixel (Fig.1).

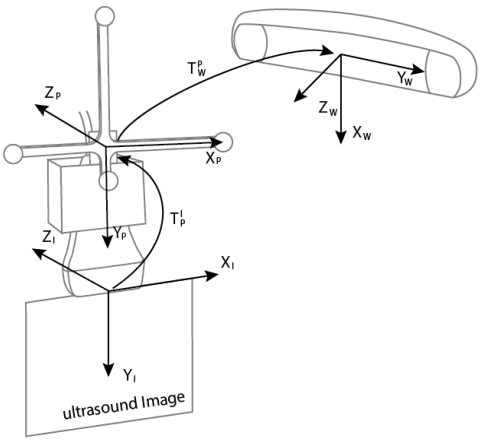

FIGURE 1. Coordinate system used in probe calibration.

Several calibration methods of ultrasonic probe tip were investigated [17]. The simplest calibration model is a target point denoted by a cross or a small sphere [12], [18]–[20]. But the limited thickness of ultrasonic beam makes the target point not always appear at the center of scan plane and this displacement can be up to several millimeters in the vertical direction. Planar calibration based on 2D planar scanning was investigated to solve the above problem [21]–[23].

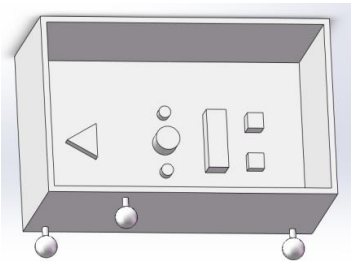

FIGURE 2. Design of calibration flume.

However the complicated boundary detection problem on plane makes the calibration process very slow, and requires complex and strict procedures for doctors as well. The Z-fiducial phantom is designed to solve the alignment problem in 2D phantoms [24]–[27], but due to the ultrasonic noises and artifacts, calibration accuracy still have an apparent influence on registration and navigation.

Aiming the above influence from ultrasonic noise and artifacts in B-mode images, this research proposed an automatic probe calibration method based on the coherent point drift (CPD) point cloud registration which incorporated the automatic extraction of contours in ultrasound images in [28]. A flume phantom has been designed and fabricated by 3D printing as the calibration tool, and the bottom has been specially designed with multiple features (Fig.2). The proposed method firstly acquires the point cloud data of a phantom's bottom utilizing an ultrasound probe, then matches the data to the point cloud from the standard model through a registration step, and finally calculates the probe parameters based on registration results. These parameters are critical for implementation of ultrasonic-based robot-assisted navigation.

II. MATERIALS AND METHODS

A. COORDINATE SYSTEMS IN ULTRASONIC NAVIGATION

In order to track pose of the spatial position of ultrasonic probe in the ultrasonic navigation, an optical or electromagnetic position sensor is often rigidly attached to the probe. Then through a series of spatial coordinate transformations, ultrasonic image, preoperative image, instrument pose are all transferred into the camera coordinate system. Fig. 1 illustrates typical coordinate systems in an ultrasonic navigation system: the world coordinate system W, the probe coordinate system P and the image coordinate system I. Transformations from I to P and from P to W are denoted as $T_{\mathrm{P}}^{\mathrm{I}}$ and $T_{\mathrm{W}}^{\mathrm{P}}$ respectively. A point in the image coordinate system and the world coordinate system are denoted as $P_{\mathrm{I}} = (u, v, 1)$ and $P_{\mathrm{W}} = (X, Y, Z, 1)$ respectively. Then the relationship between P_{I} and P_{W} can be written as

$$P_{\mathrm{W}} = T_{\mathrm{W}}^{\mathrm{P}} \cdot T_{\mathrm{P}}^{\mathrm{I}} \cdot P_{\mathrm{I}} \tag{1}$$

During image acquisition procedure, $T_{\mathrm{W}}^{\mathrm{P}}$ is calculated based on the tracking information from an external position sensor. It should be noted that each image frame has its own $T_{\mathrm{W}}^{\mathrm{P}}$.

Geometrically, points (i.e., pixels) in the B-mode ultrasound 2D image are located on a 2D rectangle in 3D space. This rectangle is represented by four parameters (depth, width, origin and direction) which can be obtained through the probe calibration. Here each of three vectors I_0, I_x, I_y contains four scalar which are used to represent the calibration results. Thus, an image coordinate P_{I} in the corresponding probe space can be written as $P_{\mathrm{P}} = I_0 + I_x u + I_y v$, or an alternative form as follows:

$$\begin{pmatrix} x \\ y \\ z \\ 1 \end{pmatrix} = T_{\mathrm{P}}^{\mathrm{I}} \begin{pmatrix} u \\ v \\ 1 \end{pmatrix} \tag{2}$$

$$T_{\mathrm{P}}^{\mathrm{I}} = \begin{pmatrix} I_y & I_x & I_0 \end{pmatrix} \tag{3}$$

B. PROBE CALIBRATION SCHEME

In the point could-based registration method, locations of points on the calibration tool is scanned by a probe and their coordinates on each image are denoted as $\{P_{1k}|k = 1, \ldots, n\}$. Similarly, the corresponding locations of probe are denoted as $\left\{T_{\mathrm{w}k}^{\mathrm{P}}|k = 1, \ldots, n\right\}$. Coordinates of points in the world coordinate system $\{P_{\mathrm{w}k}|k = 1, \ldots, n\}$ can be tracked directly and sent into (1) to get a linear system from which $T_{\mathrm{w}}^{\mathrm{P}}$ is solved. However, this method still has some limitations in application. Firstly, if the point clouds of calibration tool are too small, the features of the phantom's bottom collected by the ultrasonic probe are obviously insufficient, or they may even be recognized as noise. On the contrary, too many points in the point cloud will decrease calibration accuracy. Secondly, it is difficult to sort points, because manual sorting is time-consuming and computer sorting always results in a low success rate. Thirdly, different angles of scanning to points will produce different results when ultrasound artifacts exist.

To solve these problems, we proposed a new calibration method based on point cloud registration. The calibration tool is designed as a flume with multiple features (Fig. 2). Before calibration, we scanned the probe with reference tool using FARO Design ScanArm, a high-resolution scan arm for reverse engineering and CAD-based design, whose precision is up to 75μm. Ideally, the ultrasound image plane lies on one of the symmetrical surfaces of the probe (Fig. 3). We take the values fitted from the scanned 3D points as the initial parameters of the probe, which are $\tilde{I}_0 = (92.66, 20.56, -31.59, 1)$, $\tilde{I}_x = \left(1.123 \times 10^{-4}, -0.05910, 1.099 \times 10^{-4}, 0\right)$ and $\tilde{I}_y = (0.05911, 3.014 \times 10^{-4}, 6.443 \times 10^{-4}, 0)$. The unit of the three parameters is millimeter.

Entire calibration procedure can be divided into four steps.

Step 1: a series of ultrasonic images with corresponding probe coordinates are scanned on the phantom utilizing ultrasonic probe.

Step 2: the scattered points produced by phase feature extraction technique from all ultrasonic images are used to form the contour of flume bottom.

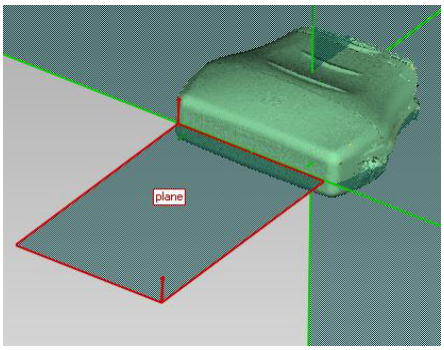

FIGURE 3. Image plane fitted from scanned points of the probe by FARO Design ScanArm.

Step 3: 3D point cloud is calculated in (1) with the initial values of probe parameters $\tilde{I}_0 = (0, 0, 0, 1)$, $\tilde{I}_x = (1, 0, 0, 0)$ and $\tilde{I}_y = (0, 1, 0, 0)$.

Step 4: transformation between the scanned point cloud and the standard model is calculated after point cloud registration. Thus, the parameters of the probe can be written as $I_0 = T_r\tilde{I}_0$, $I_x = T_r\tilde{I}_x$ and $I_y = T_r\tilde{I}_y$.

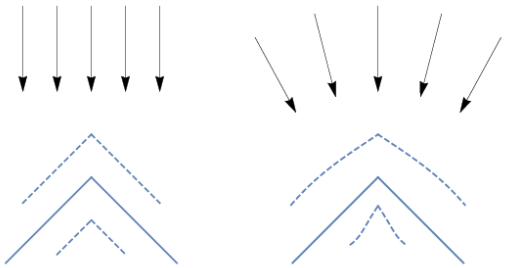

FIGURE 4. Parallel and non-parallel scan with a non-calibrated probe. (a) Scan a ridge parallelly. (b) Scan a ridge unparallelly.

Before calibration, it should be noted that the probe should be strictly moved parallel during scanning to reconstruct the surface. For example, when we parallelly scan a ridge as show in Figure 4a, even the uncalibrated probe has error along y axis (Refer to Fig. 1, i.e. actual points are either deeper or shallower than the calculated ones), the result point cloud can still preserve its original shape although it is translated; otherwise, if the probe is not parallelly moved (Fig. 4b), the result will get distorted.

C. AUTOMATIC EXTRACTION OF CONTOURS IN ULTROSNIC IMAGES

During calibration procedure, a large number of ultrasonic images are collected. Here the phase feature extraction method proposed by Chen *et al.* [27] that was originally used in surface ultrasonic image extraction, is adopted for automatic recognition. Previous experiments we conducted have shown that the ultrasonic images of the solid object in water is similar to those of the human bone surface, thus can be automatically identified by the phase feature

extraction method. Moreover, compared with the human body, ultrasound in the water has no interference from soft tissue, and its identification rate and accuracy are improved. As the probe calibration is also used for CAOS, utilization of same method in both phrases can improve accuracy and stability of the entire navigation.

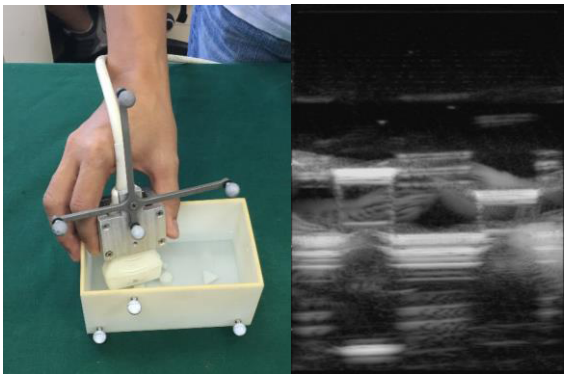

(a) (b)

FIGURE 5. Flume scanning. (a) Device setting. (b) The resulting ultrasonic image.

Fig. 5 shows a scan of the flume and the resulting ultrasonic image. In each frame, points representing the bottom surface are extracted. Point cloud data representing the bottom is then constructed after appropriate transformations to all these extracted points. Transformation from the probe coordinate system to the world coordinate system $T_{\mathrm{W}}^{\mathrm{P}}$ is calculated from the tracking information of an external position sensor Polaris Spectra (Northern Digital Inc., Canada).

Firstly, the influence of image noise and speckle to the extraction algorithm is depressed by Gaussian filtering. It is known from characteristics analysis of ultrasonic imaging that the reflector has higher amplitude in the frequency domain of image, thus the feature extraction in the frequency domain is adopted to construct the surface contour of flume bottom. Here the improved Log-Gabor wavelet is used for image detection. The 2D Log-Gabor filter on a linear frequency scale consists of two parts: the radius filter and the angle filter. Its transmission function is

$$G(\omega,\varphi)=-\frac{(\log\frac{\omega}{\omega_0})^2}{\left(2\log\frac{\sigma_\omega}{\omega_0}\right)^2}+\frac{(\varphi-\varphi_0)^2}{2\sigma_\theta^2} \tag{4}$$

where, σ_ω is the standard deviation of ω, ω_0 and φ_0 are the center frequency and the directional angle of filter respectively, σ_θ is the standard deviation of Gaussian function in the angle direction. Then 2D phase symmetry values of each point in the image can be calculated based on all 2D Log-Gabor filtering in different scales m and directions r:

$$PS(x,y)=\frac{\Sigma_r\Sigma_m\left[|e_{rm}(x,y)|-|o_{rm}(x,y)|\right]}{\Sigma_r\Sigma_m\sqrt{e_{rm}(x,y)^2+o_{rm}(x,y)^2+\varepsilon}} \tag{5}$$

D. POINT CLOUD-BASED REGISTRATION

Last step of calibration is the point cloud-based registration. Point cloud obtained on the geometric model of the calibrated flume after discretization and subdivision is taken as the reference for registration. Point cloud obtained by hand-held probe is used as the input of registration.

Currently, the main method of point cloud registration is ICP and it is a registration algorithm based on the least square criterion, which is also regarded as a generally rigid registration algorithm to compute correspondence between two sets of point clouds. However, noise and distortion exist in the extracted point cloud, making ICP fail to align it with the standard point sets.

CPD proposed by Myronenko is a probability-based registration algorithm which is suitable for both rigid and non-rigid registrations [29]. CPD method regards point set aligning as the probability density estimation problem. The reference point set is the center of the Gaussian Mixture Model (GMM). The target point set is the observation data point, and the geometric transform between the set of points is estimated by maximizing the likelihood probability of the observed data points. According to this method, the standard model point cloud of the flume here is denoted by a $M\times 3$ matrix $Y=(y_1,y_2,\ldots y_M)^{\mathrm{T}}$ and the scanned points set is denoted by a $N\times 3$ matrix $X=(x_1,x_2,\ldots x_N)^{\mathrm{T}}$. Taking Y as the centroids of GMM will produce

$$p(x)=w\frac{1}{N}+(1-w)\sum_{m=1}^{M}\frac{1}{M}p(x|m) \tag{6}$$

where, $p(x|m)=\frac{1}{(2\pi\sigma^2)^{D/2}}e^{-\frac{\|x-y_m\|^2}{2\sigma^2}}$, D is the dimension of point sets, M, N is number of points in the point sets, and $w\,(0\le w\le 1)$ represents the weight of noise points and outliers. The probability density function $p(x)$ reaches the maximum when point sets X and Y are identical. Considering the non-rigid property of ultrasound images, an affine transformation with transformation matrix B and translation t is applied to x. After variables replacement, we can get

$$p(x;B,t)=w\frac{1}{N}+(1-w)\sum_{m=1}^{M}\frac{1}{M}p(B\cdot x+t|m) \tag{7}$$

The problem is then transformed into an optimization problem. Maximizing value of the above function is equivalent to minimizing value of the negative logarithm likelihood function as

$$E\left(\theta,\sigma^2\right)=-\sum_{n=1}^{N}\log\sum_{m=1}^{M}\frac{1}{M}\frac{1}{\left(2\pi\sigma^2\right)^{D/2}}e^{-\frac{\|x_n-y_m\|^2}{2\sigma^2}} \tag{8}$$

Parameter estimation can be conducted by the expectation-maximization (EM) algorithm. The algorithm in [4] consists of two steps of iterative computation: firstly a set of parameters is used to derive the expected values of the variables, and then the maximum likelihood is estimated using these expected values. The objective function in the procedure of

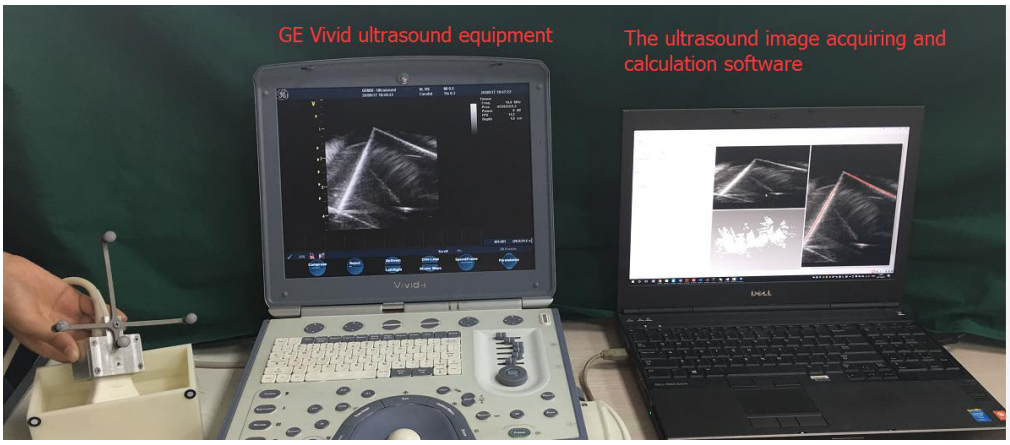

FIGURE 6. Ultrasound image acquiring and calculation procedure.

maximum likelihood estimation is as follows:

$$Q\left(\sigma^2, B, t\right) = \frac{1}{2\sigma^2}\sum_{m,n=1}^{M,N} P^{old}\left(m|x_n\right) \times \|x_n - (B \cdot y_m + t)\|^2 + \frac{3}{2}N \log \sigma^2 \quad (9)$$

In each iteration, the posteriori probability distributions $P^{old}\left(m|x_n\right)$ of mixture components are computed by using the Bayes' theorem. Then, σ^2, B, t are calculated by making partial derivatives of Q equal to zero and solve the result linear system. This is repeated until all the parameters converge.

Calculation of optimal transformation parameters based on two input matrices X, Y is the core of this calibration method. But CPD method has a defect that the result depends on the weight w in (6). The inappropriate selection of w might result in alignment failure. The practical value of w varies depending on the situation but cannot be predicted. So, we improved CPD method by adding an estimation step for w in every iteration.

To determine whether the weight parameter w is set reasonable, a certain criterion function must be selected. Obviously selecting the distance metric of the registration points as a criterion function is a proper choice. That is, calculating the Euclidean distance of a set of points X and its corresponding point Y. The optimal weight parameter w will correspond to the minimum Euclidean distance. However, in the case of actual registration, due to the existence of noise points and outliers, there will be many-to-one matching between the two set. If all the registration points are included in the calculation of the criterion function, the validity of the criterion will be affected. Therefore, only the Euclidean distance of the one-to-one match is chosen. Since the number of one-to-one matching points is different for each weight w, which we want to eliminate its influence on the criterion function, the normalized one-to-one registration point is the Euclidean distance as the final criterion function, defined as follows:

$$\frac{1}{N}\sum_{i=1}^{N} d\left(x_i, Tx_i\right)^2 \quad (10)$$

where N represents the number of one-to-one match, Tx_i is the point corresponding to x_i in Y. The estimation is done by gradient descent method. After expectation-maximization in each step, search the optimal value of w with step 0.005.

III. EXPERIMENTS AND RESULTS

A. EXPERIMENTAL EQUIPMENT

The Vivid portable ultrasonic device (GE Healthcare, USA) is adopted as the ultrasonic equipment and a reference frame for positioning is attached rigidly to the ultrasonic probe. NDI Polaris system is used as the position sensor. Features such as prism, cylinder, and cuboid, are designed and fabricated at the bottom of the flume where three cylindrical cavities with diameters of 15 mm, 20 mm and 25 mm respectively is used for validation of experimental results. The ultrasonic instrument and the position sensor are connected into a computer through the image capture card and the USB port respectively. The ultrasound image acquiring and calculation software (Fig. 6) can simultaneously trigger the ultrasonic image acquisition during position tracking of the probe.

B. EXPERIMENTAL PROCEDURE

The flume is filled by water. 40-50 ultrasonic images are collected utilizing a probe from multiple positions and viewing angles of the flume bottom and the location of probe are simultaneously recorded. Bone contour of the flume bottom in each image is extracted using the proposed automatic extraction algorithm. All these contours together with the initial parameters of probe and the NDI tracking information of each image, are used to form the data cloud in the world coordinate system.

Fifteen sets of data are collected in the experiment. On the one hand, ICP was tested for calibration, but the iteration result is not convergent. This phenomenon can be explained by the large topological difference between the scanned points and the points from model. The points of the model are evenly distributed with a relatively low density. The scanned points however, lie on some lines with high density, leaving other places empty. On another hand, the CPD method is used for calibration, and the iterative convergence results are satisfactory. Point cloud data is imported into the MATLAB

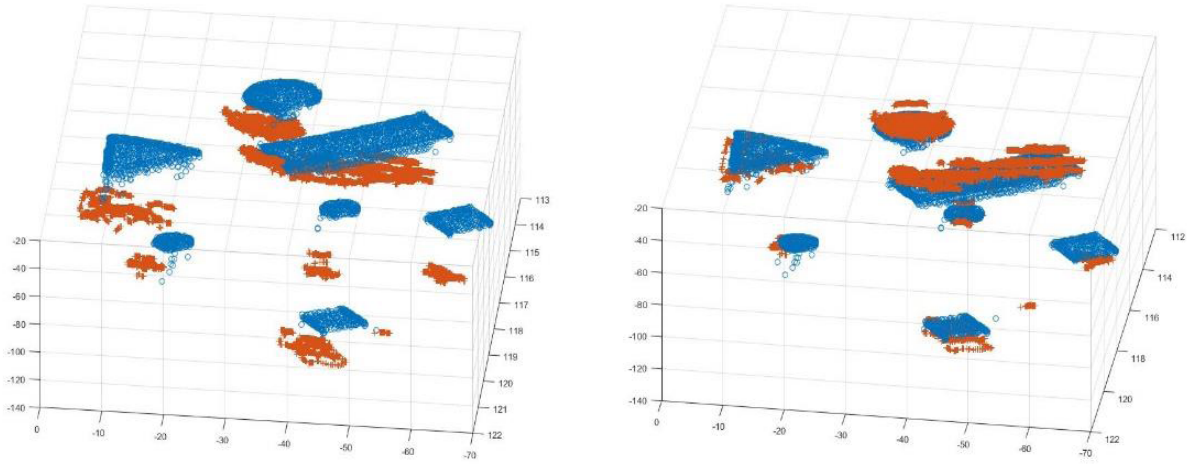

(a) (b)

FIGURE 7. CPD registration results. (a) Before registration. (b) After registration.

program for registration, and Fig. 7 shows one of CPD calibration results.

The computer used here is a workstation (DELL M4800) with a Core i7-4710MQ processor, 16GB memory, and the Microsoft Windows 10 operating system. In this condition, the average processing time of ultrasound images is about 0.8 s, and the cloud registration time is related to the number of input points. It takes 15-22 mins to finish the registration.

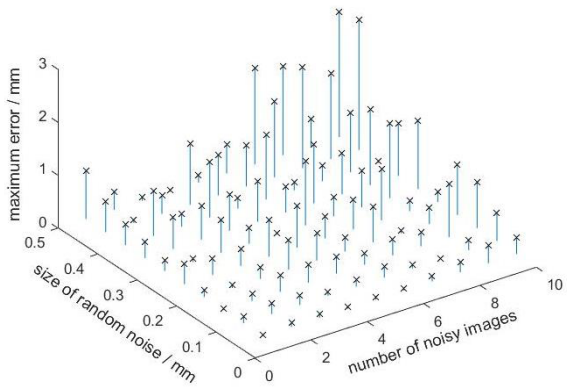

FIGURE 8. Result of robustness test.

Robustness of the proposed method is tested through adding random noise to the input. In fact, the position sensor, the ultrasonic probe, and the image processing algorithm can all become sources of noise in the point cloud. Unfortunately, they are hardly observed and measured directly. Instead, we select some of the ultrasound images and add noises to the extracted pixel or the probe's position. Then the input points are registered as usual and the results are compared with the originals. The test is repeated 10 times for each pair of selected images and noise size, and the maximum errors are recorded. Fig.8 shows the results.

FIGURE 9. Flume for calibration testing and probe for cavities measurement.

C. RESULT VERIFICATION

A tool is designed as in Fig. 9 to verify the calibration results. Cavities were scanned using an ultrasound probe. Eight images from different angle for each cavity were recorded and then fitted to a cylinder using calibrated parameters. Calibration error was determined by the displacement of center point of the cylinder's bottom and the angle of the cylinder's axis. To get the accurate value of both, a probe was used to pick the point cloud along the sides and bottom of the cavity. The cylindrical surface fitted from the side point cloud determined the axis direction, and the intersection of plane and cylindrical surface determined the coordinates of the center point.

The position errors of center points and the angular errors of axis are shown in Fig. 10 and Fig. 11 respectively. The average errors of the center point position for each cavity were 1.50 mm, 1.31 mm, 1.19 mm respectively. The average errors of the axis for each cavity were 0.85°, 0.61°, 0.99° respectively.

IV. DISCUSSION

3D ultrasound images can provide more accurate and abundant information than conventional 2D ultrasound. Based on the existed probe calibration, ultrasonic image

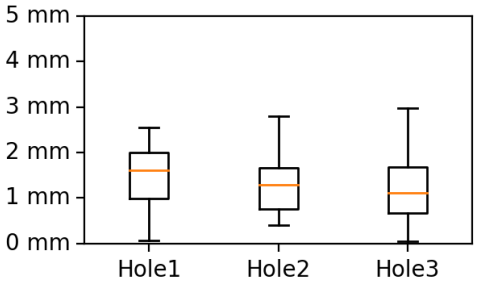

FIGURE 10. Position error of the center point.

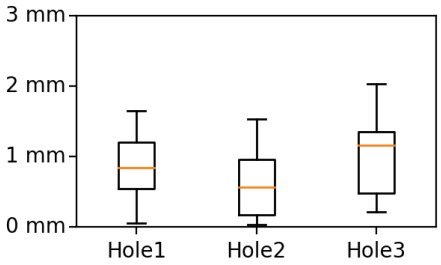

FIGURE 11. Angular error of the axis.

processing and point cloud registration algorithm, we designed and tested a new calibration method between ultrasonic probe and 3D vision device. Compared with the point cloud based registration methods adopted in [18]–[20], the proposed method is more flexible in scanning, with the only requirement that the scanning area should be covered as much as possible. Compared with the manual selection of points, automatic extraction of the outlines of calibration tool is more efficient, and more suitable for CAOS application. Although artifacts on a single ultrasound image could not be completely eliminated, calibration procedure uses the entire 3D point cloud and the registration algorithm has a certain tolerance to noise. Compared with the planar calibration methods in [21]–[23], the proposed method, which utilizes more abundant features such as prism, cylinder, and cuboid for calibration, avoids the boundary defining problem, and decreases the requirements for operator.

Because noise and distortion exist in the extracted point cloud, during the registration, ICP algorithm fail to align it with the standard point sets, which cannot achieve fully automatic calibration. Oppositely, CPD method regards point set aligning as the probability density estimation problem. The reference point set is the center of the Gaussian Mixture Model. The target point set is the observation data point, and the geometric transform between the set of points is estimated by maximizing the likelihood probability of the observed data points. But CPD method has a defect that the inappropriate selection of parameter might result in alignment failure. So we improved CPD method by adding an estimation step in every iteration. And registration could be implement successfully with high precision but not sensitive to noise. Sometimes, it still influenced by the outliers, even lead to unsuccessful registration. Fortunately, this part can be processed by hand culling, with slightly decrease in the calibration efficiency.

There are two factors influencing the confidence of the results. The first is that the accurate values of three vectors for describing the probe calibration results in the image coordinate system cannot be measured and is difficult to quantify. Here we designed a special flume model for the results verification. The cylindrical shape of cavity in the flume can be easily measured with a probe. This is a type of indirect measurement. The second is that whether the deformations in water and on human bodies are consistent is not yet determined, although we have taken into account the deformation of ultrasonic images in the proposed method. During the experimental procedure, we also found that the quality of the ultrasound images is always significantly different from the expected ones. When the probe is perpendicular to the bottom of the flume, the horizontal echo from the bottom is very strong, and the width of the strip appears in the image, but in the vertical plane it is opposite. Features such as the edge and the corner are too obvious that will have a greater impact on the image quality. In addition, materials selection and shape design of the flume are not fully optimized yet. All these problems will be investigated in the further research.

V. CONCLUSION

Combined with automatic ultrasound bone surface extraction method, the 3D ultrasonic probe calibration method based on CPD algorithm has been presented and validated in this paper. It could be used as the calibration method during orthopedics surgery navigation based on ultrasonic-CT registration. Besides, the fully automatic implementation of ultrasonic image processing and subsequent calculation is suitable for on-line calibration and verification in surgery.

REFERENCES

[1] S. Lavallée, P. Sautot, J. Troccaz, P. Cinquin, and P. Merloz, "Computer-assisted spine surgery: A technique for accurate transpedicular screw fixation using CT data and a 3-D optical localizer," *J. Image Guided Surg.*, vol. 1, no. 1, pp. 65–73, Mar. 1995.

[2] L.-P. Amiot, K. Lang, M. Putzier, H. Zippel, and H. Labelle, "Comparative results between conventional and computer-assisted pedicle screw installation in the thoracic, lumbar, and sacral spine," *Spine*, vol. 25, no. 5, pp. 606–614, Mar. 2000.

[3] A. Weidner, M. Wähler, S. T. Chiu, and C. G. Ullrich, "Modification of C1–C2 transarticular screw fixation by image-guided surgery," *Spine*, vol. 25, no. 20, pp. 2668–2673, Oct. 2000.

[4] T. Hüfner, M. Kfuri, Jr., D. Kendoff, M. Richter, J. Geerling, and C. Krettek, "Navigierte osteosynthese des proximalen femurs," *Der Unfallchirurg*, vol. 106, no. 11, pp. 975–979, Nov. 2003.

[5] D. Kendoff *et al.*, "Navigierte Iso-C^{3D}-basierte anbohrung einer osteochondralen läsion des talus," *Der Unfallchirurg*, vol. 106, no. 11, pp. 963–967, Nov. 2003.

[6] D. Kendoff, M. Citak, M. J. Gardner, T. Gösling, C. Krettek, and T. Hüfner, "Navigated femoral nailing using noninvasive registration of the contralateral intact femur to restore anteversion. Technique and clinical use," *J. Orthopaedic Trauma*, vol. 21, no. 10, pp. 725–730, Nov./Dec. 2007.

[7] D. Kendoff *et al.*, "Experimental validation of noninvasive referencing in navigated procedures on long bones," *J. Orthopaedic Res.*, vol. 25, no. 2, pp. 201–207, Feb. 2007.

[8] H. Bäthis, L. Perlick, C. Lüring, T. Kalteis, and J. Grifka, "CT-basierte und CT-freie navigation in der knieendoprothetik: Ergebnisse einer prospektiven studie," *Der Unfallchirurg*, vol. 106, no. 11, pp. 935–940, Oct. 2003.
[9] C. R. Maurer, Jr., *et al.*, "AcouStick: An optically tracked A-mode ultrasonography system for registration in image-guided neurosurgery," *Stereotact. Funct. Neurosurg.*, vol. 72, nos. 2–4, pp. 143–144, Apr. 2000.
[10] C. Amstutz *et al.*, "A-mode ultrasound-based registration in computer-aided surgery of the skull," *Arch. Otolaryngol. Head Neck Surg.*, vol. 129, no. 12, pp. 1310–1316, Dec. 2003.
[11] A. Mozes, T.-C. Chang, L. Arata, and W. Zhao, "Three-dimensional a-mode ultrasound calibration and registration for robotic orthopaedic knee surgery," *Int. J. Med. Robot.*, vol. 6, no. 1, pp. 91–101, Mar. 2010.
[12] A. Brounstein, I. Hacihaliloglu, P. Guy, A. Hodgson, and R. Abugharbieh, "Towards real-time 3D US to CT bone image registration using phase and curvature feature based GMM matching," in *Proc. MICCAI*, 2011, pp. 235–242.
[13] J. Kowal, C. Amstutz, F. Langlotz, H. Talib, and M. G. Ballester, "Automated bone contour detection in ultrasound B-mode images for minimally invasive registration in computer-assisted surgery—An *in vitro* evaluation," *Int. J. Med. Robot.*, vol. 3, no. 4, pp. 341–348, Dec. 2007.
[14] W. Wein, A. Karamalis, A. Baumgartner, and N. Navab, "Automatic bone detection and soft tissue aware ultrasound–CT registration for computer-aided orthopedic surgery," *Int. J. Comput. Assist. Radiol. Surg.*, vol. 10, no. 6, pp. 971–979, Jun. 2015.
[15] D. C. Barratt *et al.*, "Self-calibrating 3D-ultrasound-based bone registration for minimally invasive orthopedic surgery," *IEEE Trans. Med. Imag.*, vol. 25, no. 3, pp. 312–323, Mar. 2006.
[16] D. C. Barratt *et al.*, "Instantiation and registration of statistical shape models of the femur and pelvis using 3D ultrasound imaging," *Med. Image Anal.*, vol. 12, no. 3, pp. 358–374, Jun. 2008.
[17] S. W. Hughes *et al.*, "Volume estimation from multiplanar 2D ultrasound images using a remote electromagnetic position and orientation sensor," *Ultrasound Med. Biol.*, vol. 22, no. 5, pp. 561–572, 1996.
[18] P. R. Detmer *et al.*, "3D ultrasonic image feature localization based on magnetic scanhead tracking: *In vitro* calibration and validation," *Ultrasound Med. Biol.*, vol. 20, no. 9, pp. 923–936, 1994.
[19] M. J. Gooding, S. H. Kennedy, and J. A. Noble, "Temporal calibration of freehand three-dimensional ultrasound using image alignment," *Ultrasound Med. Biol.*, vol. 31, no. 7, pp. 919–927, Jul. 2005.
[20] D. V. Amin *et al.*, "Calibration method for determining the physical location of the ultrasound image plane," in *Proc. MICCAI*, 2001, pp. 940–947.
[21] R. W. Prager, R. N. Rohling, A. H. Gee, and L. Berman, "Rapid calibration for 3-D freehand ultrasound," *Ultrasound Med. Biol.*, vol. 24, no. 6, pp. 855–869, Jul. 1998.
[22] F. Rousseau, P. Hellier, and C. Barillot, "Confhusius: A robust and fully automatic calibration method for 3D freehand ultrasound," *Med. Image. Anal.*, vol. 9, no. 1, pp. 25–38, Feb. 2005.
[23] P.-W. Hsu, R. W. Prager, A. H. Gee, and G. M. Treece, "Rapid, easy and reliable calibration for freehand 3D ultrasound," *Ultrasound Med. Biol.*, vol. 32, no. 6, pp. 823–835, Jun. 2006.
[24] R. M. Comeau, A. Fenster, T. M. Peters, "Integrated MR and ultrasound imaging for improved image guidance in neurosurgery," *Proc. SPIE*, vol. 3338, pp. 747–754, Jun. 1998, doi: 10.1117/12.310954.
[25] N. Pagoulatos, D. R. Haynor, and Y. Kim, "A fast calibration method for 3-D tracking of ultrasound images using a spatial localizer," *Ultrasound Med. Biol.*, vol. 27, no. 9, pp. 1219–1229, Sep. 2001.
[26] L. G. Bouchet, S. L. Meeks, G. Goodchild, F. J. Bova, J. M. Buatti, and W. A. Friedman, "Calibration of three-dimensional ultrasound images for image-guided radiation therapy," *Phys. Med. Biol.*, vol. 46, no. 2, pp. 559–577, Feb. 2001.
[27] T. K. Chen, P. Abolmaesumi, A. D. Thurston, and R. E. Ellis, "Automated 3D freehand ultrasound calibration with real-time accuracy control," in *Proc. MICCAI*, 2006, pp. 899–906.
[28] I. Hacihaliloglu, R. Abugharbieh, A. J. Hodgson, and R. N. Rohling, "Bone surface localization in ultrasound using image phase-based features," *Ultrasound Med. Biol.*, vol. 35, no. 9, pp. 1475–1487, Sep. 2009.
[29] A. Myronenko and X. Song, "Point set registration: Coherent point drift," *IEEE Trans. Pattern Anal. Mach. Intell.*, vol. 32, no. 12, pp. 2262–2275, Dec. 2010.

LIFENG WANG was born in Ordos, Inner Mongolia, China, in 1980. He received the B.S. and M.S. degrees in mechanical engineering and automation from Beihang University, Beijing, in 2003 and 2006.

From 2006 to 2010, he was a Senior Engineer and an Architect with the Toshiba (China) Medical Research and Development Center. From 2011 to 2012, he was a Manager with Sinopharm Medicine Holding Beijing Huahong Co., Ltd. Since 2013, he has been with Beihang University for the Ph.D. research.

Mr. Wang participated in core research of the first modular orthopedic surgery robot system in China, the first study of ENT robot in China, and the first study of dental implant robot in China. His research interests include surgical navigation, medical image computing, and scientific visualization.

TIANMIAO WANG received the B.S. degree in electronic engineering from Xi'an Jiaotong University, in 1982, and the M.S. and Ph.D. degrees from Northwestern Polytechnical University, Xi'an, in 1987 and 1990, respectively.

He was a Post-Doctoral Scholar with the Department of Computer Science, Tsinghua University from 1990 to 1992 and with the Rizzoli Orthopaedic Institute, Italy, from 1992 to 1995. Since 1995, he has been a Professor with the Robotics Institute, Beihang University. His research interests include medical robotics and embedded mechatronics.

Dr. Wang is the Chair of the IEEE Robotics and Automation Society Beijing Chapter. He was a recipient of the two Second Class Prizes of the National Science and Technology Progress Award of China, in 2008 and 2015, respectively.

HONGPENG LIU was born in Dongying, Shandong, China, in 1992. He received the B.S. degree in mathematics from Beihang University, Beijing, in 2015, where he is currently pursuing the M.S. degree in mechatronic engineering from the Robotics Institute.

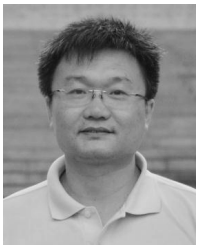

LEI HU received the B.S. and M.S. degrees in mechanical engineering and automation from Beihang University, Beijing, in 1986 and 2007, respectively, and the Ph.D. degree from Harbin Engineering University, Harbin, in 2015.

He is currently a Senior Engineer with the School of Mechanical Engineering and Automation, Beihang University. His research interests include medical robot, mechanical design, and mechatronics.

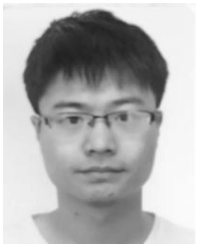

ZHONGHAO HAN was born in Xinzhou, Shanxi, China, in 1994. He received the B.S. degree in mechanical engineering and automation from Beihang University, Beijing, China, in 2016, where he is currently pursuing the master's degree. His research interests include medical robot, ultrasound inspection, and medical image processing.

WENYONG LIU received the B.S. degree in mechanical engineering from the North China University of Science and Technology, Tangshan, China, in 1998, and the Ph.D. degree in mechatronics from Beihang University, Beijing, China, in 2009.

From 1998 to 2000, he was an Assistant Engineer with the Changshan Textile Co., Ltd, Hebei. Since 2009, he has been an Assistant Professor with the School of Biological Science and Medical Engineering, Beihang University. His research interests include medical robotics and computer assisted surgery.

NA GUO was born in Yuncheng, Shanxi, China, in 1988. She received the B.S. degree in automation from University of Science and Technology Beijing, Beijing, in 2009, and the M.S. degree in mechanical engineering and automation from Beihang University, Beijing, in 2012.

From 2012 to 2015, she was an Engineer with the Beijing General Research Institute of Mining and Metallurgy. From 2015 to 2016, she was a Development Manager with Beijing DKJ Medical Technology Co., Ltd. Since 2015, she has been with Beihang University for the Ph.D. research.

YANSONG QI received the Ph.D. degree from Peking University, Beijing, in 2017.

From 2003, he was an Orthopedist with the Department of Orthopedics, Inner Mongolia People's Hospital, China. His research interests include ACL reconstructions, personalized artificial knee prosthesis, biomechanics, and 3-D printing technology in orthopedics.

YONGSHENG XU received the Ph.D. degree in osteopathy from the Medical School of Chinese PLA, Beijing, in 2012. From 2003, he was an Orthopedist with the Department of Orthopedics, Inner Mongolia People's Hospital, China. He is currently the Director with the Inner Mongolia Autonomous Region Sports Medicine Center and the Chief of Surgery with Inner Mongolia People's Hospital. His research interests include revision surgery of artificial joint replacement, arthroscopic treatment of shoulder, elbow, knee and ankle injuries.